Phase diagram and optimal control for n-tupling discrete time crystal

Arkadiusz Kuroś[1], Rick Mukherjee[2], Weronika Golletz[1], Frederic Sauvage[2], Krzysztof Giergiel[1], Florian Mintert[2] and Krzysztof Sacha[1]

[1] Instytut Fizyki Teoretycznej, Uniwersytet Jagielloński, ulica Profesora Stanisława Łojasiewicza 11, PL-30-348 Kraków, Poland
[2] Blackett Laboratory, Imperial College London, SW7 2AZ, UK

E-mail: `arkadiusz.kuros@uj.edu.pl`

Abstract. A remarkable consequence of spontaneously breaking the time translational symmetry in a system, is the emergence of time crystals. In periodically driven systems, discrete time crystals (DTC) can be realized which have a periodicity that is n times the driving period. However, all of the experimental observations have been performed for period-doubling and period-tripling discrete time crystals. Novel physics can arise by simulating many-body physics in the time domain, which would require a genuine realisation of the n-tupling DTC. A system of ultra-cold bosonic atoms bouncing resonantly on an oscillating mirror is one of the models that can realise large period DTC. The preparation of DTC demands control in creating the initial distribution of the ultra-cold bosonic atoms along with the mirror frequency. In this work, we demonstrate that such DTC is robust against perturbations to the initial distribution of atoms. We show how Bayesian methods can be used to enhance control in the preparation of the initial state as well as to efficiently calculate the phase diagram for such a model. Moreover, we examine the stability of DTCs by analyzing quantum many-body fluctuations and show that they do not reveal signatures of heating.

1. Introduction

Ever since the original conception of a time crystal in quantum many-body systems [1], there has been a growing interest to understand these objects theoretically [2–17] as well as to realise them experimentally [18–23]. It turns out that in the model proposed in [1] such symmetry breaking cannot be observed if a system is initially in the ground state [24], while excited-state realizations are allowed [25]. Furthermore, time crystals cannot be observed for systems in the presence of long-range power-law interaction in their equilibrium state [26, 27]. However, recent study shows [28] that the time crystal behaviour can also be observed in the ground state of a system with long-range interactions in the form of spin strings which are hard to realize in real experiments [29].

Popular realisations of time crystals involving excited states are DTCs which arise in periodically driven many-body systems. In such systems, the discrete temporal symmetry can be broken as a result of the inter-particle interactions. The first proposal of DTC involved a bouncing gas of ultra-cold atoms [2] and latter proposals involved spin-1/2 systems [3,4]. So far, the experimental realization of DTC has been performed in trapped ions [18] and nitrogen-vacancy centres in a diamond [19], where period-doubling DTC and period-tripling DTC was observed respectively (see also [20–23]). Although there are few theoretical models to realize period n-tupling DTC [11, 30–33], where $n > 3$, there has yet been no experimental observation of them.

In this work, we study a model of ultra-cold bosonic atoms bouncing resonantly on an oscillating mirror [2] which has the potential of realizing n-tupling DTC, where n can be arbitrarily large. The motivation to physically realise n-tupling DTC lies in the fact that they provide a suitable platform to exhibit topological time crystals [34, 35], temporal quasi-crystals [33, 36–39] as well as to demonstrate various nontrivial condensed-matter phenomena in the time domain [11, 40–45]. However, the experimental realization of this model involves multiple challenges as detailed in [11, 46].

The formation of DTC in the system occurs due to sufficiently strong attractive interaction between atoms and it can be observed if an initial state is properly located with respect to the mirror position [11]. This requires a precise system control which cannot be guaranteed in each experimental realization. By evaluating the phase diagrams of this model, we examine the robustness of the DTC against perturbations of the initial atomic distribution. Moreover, we theoretically investigate the possibility of applying optimal control based on Bayesian optimization which could be performed on the experimental realisations of DTCs. We also address the question if the DTCs are stable against quantum many-body fluctuations which can result in heating of the system. Although the model we study allows arbitrarily large n, as a proof of principle, thorough analysis for period-doubling and period-quadrupling DTCs are addressed in this work. This will be hugely beneficial for real experiments which will most likely be carried out with a larger n to reduce possible atom losses.

The paper is organized as follows. In Section 2 we present the system of ultra-cold bosonic atoms bouncing on an oscillation atom mirror. The results concerning the phase diagrams and optimal control are shown in Section 3 and Section 4, respectively, while quantum many-body fluctuations of DTCs is presented in Section 5.

2. Theory: Model for period n-tupling discrete time crystal

We consider N ultra-cold bosonic atoms which are bouncing resonantly on an oscillating atom mirror. We assume that the system is strongly confined in the transverse directions and can be treated within the one-dimensional approximation. Atoms interact with each other via a contact potential whose strength g_0 is proportional to the s-wave scattering length and can be controlled by means of the Feshbach resonance mechanism [47]. We restrict the discussion to attractive interactions $g_0 < 0$. The system can be effectively

described by a Bose-Hubbard model, Eq. (4), which is schematically presented in Fig. 1f. It turns out that for sufficiently strong attractive interactions, the system spontaneously breaks discrete time translation symmetry of the Hamiltonian and starts evolving with a period n-times longer than the period of the Hamiltonian (see Fig. 1a-e). Before describing the many-body phenomena in detail, it is useful to discuss the single-particle picture in order to better understand the concept of resonant driving in this model.
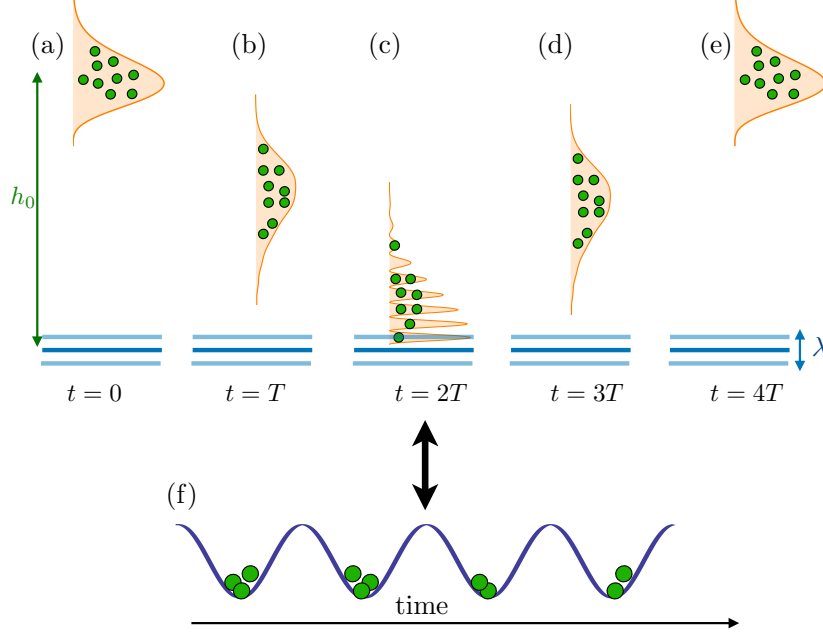
Figure 1. Setup figure of bouncing atoms on an oscillating mirror with period T for an $n : 1$ resonant driving where $n = 4$. (a) The initially prepared atomic distribution at the classical turning point h_0 returns to the starting position at $t = 4T$ (e). Figures (b)-(d) show the atomic distribution for time $t = T$, $t = 2T$ and $t = 3T$, respectively. (f) In the effective description, the system is described by Bose-Hubbard model, see (4).

2.1. Single particle problem

Consider a classical particle bouncing on an oscillating mirror with frequency ω and amplitude proportional to λ in the presence of a gravitational field. The Hamiltonian of the system in the frame moving with the mirror and in gravitational units has the form [2, 11, 48–50]

$$H_0(z, p, t) = \frac{p^2}{2} + z + \lambda z \cos \omega t, \quad z \geq 0. \tag{1}$$

For $\lambda = 0$, the system is integrable and its motion is periodic with frequency $\Omega = \partial H_0(I)/\partial I$, where $H_0(I) = (3\pi I)^{2/3}/2$ is the unperturbed part of the Hamiltonian (1) in the action-angle variables [11, 49–51]. In this picture, I is the classical analogue of the energy quantum number for an unperturbed particle. The distance of the mirror from the classical turning point is related to the frequency via the relation $h_0 = \pi^2/(2\Omega^2)$.

In the presence of small mirror oscillations ($\lambda \ll 1$), we are interested in the motion of a particle sufficiently close to a periodic orbit that is resonant with the driving, i.e., $\omega = n\Omega$, where n is an integer number. Because of the periodicity in time of the system, in the quantum description we can define the Floquet Hamiltonian $H = H_0 - i\partial_t$ which possesses T-periodic eigenstates (where $T = 2\pi/\omega$) known as Floquet states [49, 50]. To describe the motion of a particle close to the $n : 1$ resonant orbit one can apply the secular approximation [11, 49–52]. The resulting secular Hamiltonian indicates that in the frame moving along a resonant orbit, an atom behaves effectively like a particle in a periodic time-independent lattice potential with n sites and periodic boundary conditions and for $n \to \infty$ a band structure in the quasi-energy spectrum emerges [11, 40, 53–56]. We only consider the first quasi-energy band, therefore we construct n Wannier functions $w_i(z, t)$ localized in different sites of the periodic effective potential [11, 40]. These Wannier functions, in the laboratory frame, are localized wavepackets $w_i(z, t)$ moving along a classical resonant orbit with period nT. Now we switch from single particle to ultra-cold atoms which fulfil an $n : 1$ resonance condition with the mirror motion.

2.2. Cloud of ultra-cold atoms

The many-body Floquet Hamiltonian of ultra-cold bosonic atoms which are bouncing resonantly on an oscillating atom mirror, in the Hilbert subspace of (nT)-periodic states, can be written in the form [2, 11, 40]

$$\hat{\mathcal{H}} = \frac{1}{nT} \int_0^{nT} dt \int_0^{\infty} dz \, \hat{\Psi}^\dagger \left[H_0 + \frac{g_0}{2} \hat{\Psi}^\dagger \hat{\Psi} - i\partial_t \right] \hat{\Psi}, \tag{2}$$

where H_0 is the single-particle Hamiltonian (1) and $\hat{\Psi}$ is the bosonic field operator. For a BoseEinstein condensate (BEC) all atoms occupy the same single-particle state and the many-body wave-function factorizes as $\phi_0(z_1, t)\phi_0(z_2, t)...\phi_0(z_N, t)$. In the mean-field approximation $\phi_0(z, t)$ is a solution of the GrossPitaevskii (GP) equation [47]

$$i\partial_t \phi_0(z, t) = \left[\frac{p^2}{2} + z + \lambda z \cos \omega t + g_0 N |\phi_0(z, t)|^2 \right] \phi_0(z, t). \tag{3}$$

In order to get intuition about solutions of the GP equation that describe resonant motion of atoms let us restrict the analysis to the resonant single-particle Hilbert subspace spanned by the n localized Wannier wavepackets $w_i(z, t)$ of the first quasi-energy band of the $n : 1$ resonantly driven system (1), see [2, 11, 40] for details. The mean-field energy functional corresponding to the many-body Floquet Hamiltonian (2), in the Wannier basis $\phi_0(z, t) = \sum_{i=1}^n a_i w_i(z, t)$, has the form

$$E = -\frac{J}{2} \sum_{i=1}^n (a_{i+1}^* a_i + c.c.) + \frac{N}{2} \sum_{i,j=1}^n U_{ij} |a_i|^2 |a_j|^2, \tag{4}$$

where $J = -\frac{2}{nT} \int_0^{nT} dt \int_0^\infty dz \; w_{i+1}^*(z,t)[H_0 - i\partial_t]w_i(z,t)$ is the tunneling amplitude of atoms between neighboring Wannier wavepackets while $U_{ij} = \frac{2g_0}{nT} \int_0^{nT} dt \int_0^\infty dz \; |w_i(z,t)|^2 |w_j(z,t)|^2$ for $i \neq j$ and $U_{ii} = \frac{g_0}{nT} \int_0^{nT} dt \int_0^\infty dz \; |w_i(z,t)|^4$ describe the strength of the effective interactions between atoms. This energy E is actually the mean-field quasi-energy per particle. Extrema of E are given by solutions of the GP equation (3) and can be found analytically for the case $n = 2$ [2], and numerically for $n > 2$. It turns out that if the strength of the attractive interactions is smaller than a certain critical value, i.e. $|g_0 N| < |g_{cr} N|$, the mean-field solution corresponding to the minimal energy E is of the form $\phi_0(z,t) = (1/\sqrt{n}) \sum_{i=1}^n w_i(z,t)$ [2]. However, when the interaction strength is larger than the critical value $|g_{cr} N|$, $\phi_0(z,t)$ is not a uniform superposition of $w_i(z,t)$, which means that the system chooses a periodic solution evolving with the period n times longer than the period expected from the symmetry of the Hamiltonian (see Fig. 1 for the case $n = 4$). The discrete time translation symmetry is broken and a period n-tupling time crystal phase forms. The solution for sufficiently large interaction is given by the single wavepacket $\phi_0(z,t) \approx w_i(z,t)$. For this reason it is much better to realize the experiment in the regime $|g_0 N| \gg |g_{cr} N|$ [11].

2.3. Challenges in the realization of a period n-tupling DTC

In this subsection we discuss the most important challenges in the realization of a period n-tupling DTC by means of ultra-cold atom system bouncing on the oscillating mirror. In the laboratory it could be difficult to realize the hard-wall mirror that we have assumed in all theoretical analyses. However, if a realistic Gaussian shape mirror (that can be produced by a repulsive light-sheet) is used, the same time crystal phenomena can be realized as in the hard-wall case. [46].

In the experimental realization of a DTC, the initial distribution of BEC will be prepared as a harmonic oscillator ground state matching the Wannier state at a classical turning point [11]. However, the preparation of this initial atomic distribution is subject to experimental imperfections. For example, the atomic cloud released from the harmonic trap may have non-zero initial momentum, can be displaced from the classical turning point and may have non-Gaussian shape. The displacement of the cloud introduces detuning of bouncing gas of atoms from the resonant driving by the oscillating mirror. Moreover, there are typically shot-to-shot fluctuations in the position of the atoms in subsequent repetitions of an experiment. We expect that a sufficiently strong attractive interaction between atoms will compensate small displacements of the initial position of the wavepacket from the classical turning point. To show the robustness of DTC against perturbations of the initial atomic distribution, we determine the phase diagram as a function of displacement and interaction strength. However, if the displacement parameter is larger than the critical value and the initial position is not stable the mirror frequency needs to be corrected. For determining the optimal mirror frequency we have used the Bayesian optimization method.

It is also important to take into account the potential heating sources as well as

possible atomic losses occurring in the system. Hence, we examine the stability of DTC on a long time scale against quantum many-body fluctuations which can result in heating of the system. In order to reduce atomic losses, it is better to choose a higher ratio of response period to driving period [11]. For a larger value of n the numerical simulations are time consuming. Therefore we also discuss the Bayesian optimization in the context of reducing numerical cost which would be essential for potential experiments, where a higher n is required [11, 46].

3. Constructing the phase diagram for period-doubling and period-quadrupling discrete time crystals

We investigate the robustness of DTCs with regards to imperfect preparation of the initial state of the BEC. We start from an initial state which is the optimal Gaussian approximation of the mean-field solution of the DTC located exactly at the classical turning point h_0 above the mirror

$$\phi_0(z, t = 0) = \left(\frac{\tilde{\omega}_0}{\pi}\right)^{1/4} e^{-\tilde{\omega}_0(z-h_0)^2/2}. \tag{5}$$

The parameter $\tilde{\omega}_0$ is the frequency of the harmonic trap where the BEC is initially prepared and it is chosen such that the width of the atomic cloud matches the width of the Wannier wavepacket $w_i(z, t)$ at the classical turning point [11]. We consider an $n : 1$ resonant driving of atoms by an oscillating atom mirror (see Sec. 2.1). Spontaneous breaking of the discrete time translation symmetry of the system, and consequent formation of the DTC, occurs for sufficiently strong attractive boson-boson interactions [2, 11]. Then, the initially prepared wavepacket (5) is expected to be returning to the vicinity of the initial position after each period nT, as one can observe for the case $n = 4$ in Fig. 1.

It is convenient to introduce the quantum fidelity function

$$F(t) = |\langle\phi_0(0)|\phi_0(t)\rangle|^2, \tag{6}$$

where $\phi_0(t)$ is the solution of the GP equation (3). Such a quantity can be recovered from an average particle-number distribution which can by measured as long as the overlap $\langle w_1(t)|w_2(t)\rangle \approx 0$ at the measurement time t. The fidelity (6) for $n = 2$ (thus for the period-doubling DTC) and for sufficiently strong attraction is presented in Fig. 2b. The Fourier transform of $F(t)$ shows a single peak located at the half driving frequency $\omega/2$ (Fig. 2d). This peak is related to the subharmonic response of the system which is the signature of the period-doubling time crystal [5]. However, for weak attractive interactions (which correspond to the symmetry preserving regime) after the tunneling time $t = \pi/J \gg T$ we observe transfer of atoms to the second wavepacket (Fig. 2a) which evolves along the same $2 : 1$ resonant trajectory and is delayed (or advanced, depending on the point of view) by T with respect to the initial wavepacket. After another period π/J, atoms tunnel back to the initial wavepacket and this dynamics continues with
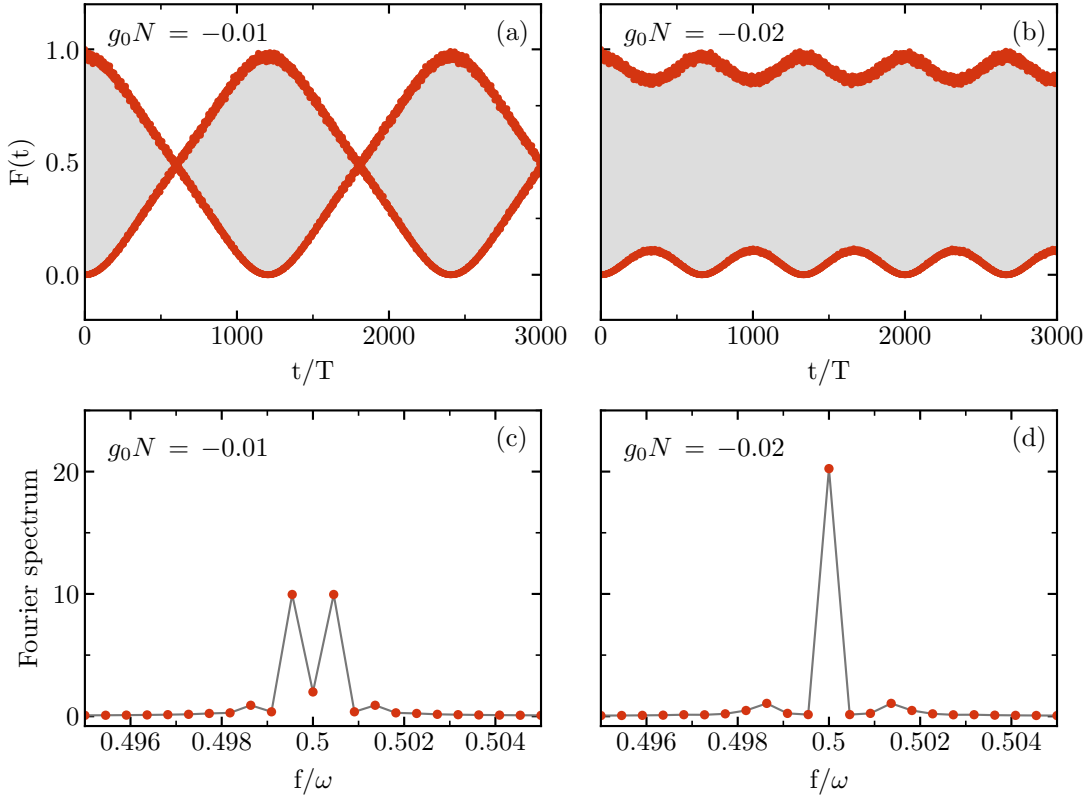
Figure 2. Period-doubling DTC ($n = 2$). Top panels: Quantum fidelity (6) obtained for the initial state (5) as a function of t/T for $g_0 N = -0.01$ (a) and $g_0 N = -0.02$ (b). In (a), the evolution of the fidelity reveals beating which is related to tunneling of atoms between two Wannier wavepackets $w_{1,2}(z, t)$ that evolve along the $2 : 1$ resonant orbit. The beating period corresponds to the tunneling period π/J where $J = 7.26 \times 10^{-4}$. Bottom panels: Fourier transform of the fidelity obtained at the stroboscopic time $t = T, 2T, 3T...$ for $g_0 N = -0.01$ (c) and $g_0 N = -0.02$ (d). One can observe the peaks of the Fourier transform located at $f = \omega/2$ for $|g_0 N| \gg |g_{cr} N|$, where $g_{cr} N \approx -0.011285$. The parameters of the initial state (5) are: $\tilde{\omega}_0 = 0.68$ and $h_0 = 9.82$ and the frequency and the amplitude of the mirror oscillations are $\omega = 1.4$ and $\lambda = 0.12$, respectively.

period $2\pi/J$. Consequently, the Fourier transform of the fidelity function (6) reveals splitting of the Fourier peak around $\omega/2$ (Fig. 2c). Such two separated peaks in the frequency domain are consistent with the beating in the plot of $F(t)$. Note that the decay of the $(2T)$-periodic evolution due to tunneling of non-interacting atoms takes place even if there is no detuning from the resonant driving. It is in contrast to DTCs in spin systems where in the absence of any detuning from the perfect spin flip, time evolution of the spin systems is still periodic with period $2T$ [3–5, 18–21].

As mentioned in Sec. 2.3 various experimental imperfections may cause fluctuations in the average momentum of atoms and of the frequency of the harmonic trap where the atomic cloud is initially prepared. Hence, we consider the initial states

$$\phi_0(z, t = 0) = \left(\frac{\tilde{\omega}}{\pi}\right)^{1/4} e^{-\tilde{\omega}(z-h)^2/2 - ip_0(z-h)}, \qquad (7)$$

where the initial average momentum p_0 and the frequency $\tilde{\omega}$ are sampled from the uniform distributions in the intervals $(-\delta p_0, \delta p_0)$ and $(\tilde{\omega}_0 - \delta\tilde{\omega}_0, \tilde{\omega}_0 + \delta\tilde{\omega}_0)$, respectively. Furthermore the initial location of the wavepacket (7) is taken to be $h = h_0 + \epsilon$, where the displacement parameter ϵ denotes the detuning of the system from a perfect resonant driving. This displacement parameter ϵ and the interaction strength $g_0 N$ constitute the space of parameters for which we determine the phase diagram of the DTC. We expect that even if $\epsilon \neq 0$, sufficiently strong interactions are able to stabilize the evolution of the DTC.
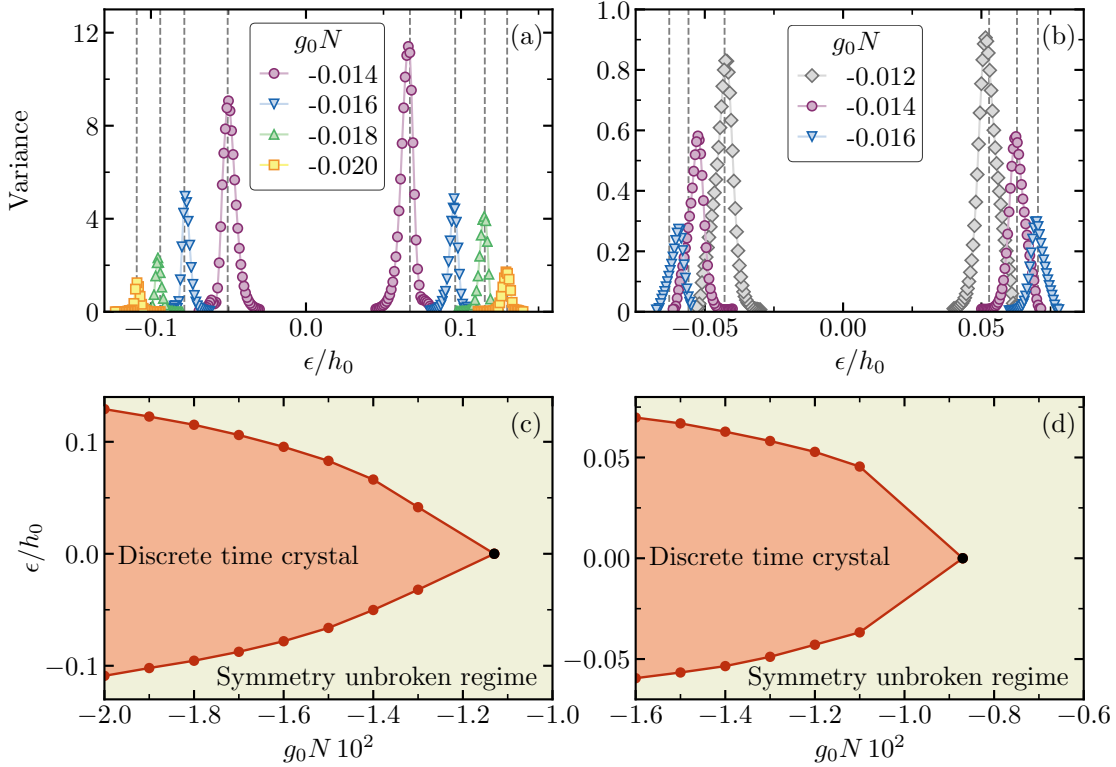
Figure 3. Period-doubling ($n = 2$) and period-quadrupling ($n = 4$) DTCs. Top panels: Variance of the Fourier peak magnitude as a function of displacement parameter ϵ for different values of $g_0 N$ (given in the legend) with $n = 2$ (a) and $n = 4$ (b). Bottom panels: Phase diagram of DTC in displacement parameter ϵ and interacting strength $g_0 N$ phase space with $n = 2$ (c) and $n = 4$ (d). The black dots correspond to the perfect $\epsilon = 0$ case, see Sec. 2.2. In the $n = 2$ case, the parameters are the following: $\omega = 1.4$, $\lambda = 0.12$, $h_0 = 9.82$, $\tilde{\omega}_0 = 0.68$ while p_0 and $\tilde{\omega}/\tilde{\omega}_0$ in (7) are uniformly drawn in the intervals $[-0.1, 0.1]$ and $[0.98, 1.02]$, respectively. In the $n = 4$ case, we have: $\omega = 1.79$, $\lambda = 0.12$, $h_0 = 24.44$, $\tilde{\omega}_0 = 0.5$, $p_0 \in [-0.05, 0.05]$ and $\tilde{\omega}/\tilde{\omega}_0 \in [0.98, 1.02]$.

To determine the critical value of ϵ for a given $g_0 N$, we analyze the fluctuations of the amplitude of the peak at $\omega/2$ (for period-doubling DTC) and at $\omega/4$ (for period-quadrupling DTC) in the Fourier transform of the fidelity (6) obtained in m random realizations of (7). We expect that the largest fluctuations of the peak amplitude can be observed near the critical point between the DTC regime and the symmetry unbroken

regime [5]. Indeed, the variance of the peak amplitude shows a strong maximum at the critical point as clearly visible in Fig. 3a-b. Performing numerical simulations for different values of $g_0 N$ we obtain the phase diagram depicted in Fig. 3c for the period-doubling DTC. Similar phase diagram but for the period 4-tupling DTC is shown in Fig. 3d. In the latter case the maximum of the variance of the amplitude of the Fourier peak at $\omega/4$ is used as the signature of the critical point. One can see that the phase diagrams are not symmetric with respect to $\epsilon = 0$. It shows that the displacement with the case $h > h_0$ is favorable for the formation of a DTC, compared to the case $h < h_0$. This is a consequence of the influence of the gravitational field. It should be noticed that the above approach is used in the regime where the symmetry breaking state is approximately given by a single wavepacket. Close to $g_{cr} N$, the symmetry breaking states are superposition of two wavepackets with unequal weights. Therefore, in order to obtain $g_{cr} N$, indicated by black dots in phase diagrams Fig. 3c-d, we have used the two-mode approximation (4).

In order to reduce the numerical burden, locating the critical ϵ, corresponding to a maximum of the variance, was turned into an optimization problem for which we have applied Bayesian optimization (see Appendix A). The positions of the variance peaks predicted at the end of the optimizations are marked by the dashed vertical lines in Fig. 3a-b. Using Bayesian optimization for 15 iterations to obtain the phase diagrams in Fig. 3c-d we have reduced by tenfold the computational time with efficiency around 70%.

4. Optimal control of the distance of the atomic cloud to the mirror

In an experimental realization of a DTC, the true distance h to the mirror may deviate more than the critical ϵ from h_0 (see Sec. 3) and will fluctuate around an average value $\bar{h}$ in between each realization. Here we show that the mirror oscillations frequency could be adjusted, directly onto the experiment, to best account for this unknown average value $\bar{h}$.

For that purpose, we resort to Bayesian optimization in order to optimize the mirror frequency which allows one to control the true distance h. In the following we assume that the atomic cloud is prepared at a distance h randomly chosen, at each realization, from the uniform distribution in the range $[\bar{h} - \delta h, \bar{h} + \delta h]$. Because we do not know $\bar{h}$ we choose the frequency $\tilde{\omega}_0$ of the harmonic trap optimal for h_0. Furthermore, $\bar{h}$ is taken to be such that $\bar{h} - h_0 \approx 0.3 h_0 \gg \delta h$. In practice it is important to ensure that $\bar{h}$ is above h_0 because if $\bar{h} - h_0 < -0.1 h_0$, there is significant overlap of $\phi_0(z, 0)$ with more than one Wannier state limiting the optimization procedure. To define the optimization problem one needs to specify a figure of merit to be maximized. In this case it is taken to be the fidelity function

$$F(\omega) = |\langle \phi_0(0) | \phi_0(nT) \rangle|^2, \tag{8}$$

obtained after n periods of the mirror oscillations $T = 2\pi/\omega$, where $\phi_0(z, t = 0)$ is given in (7). At each step of the optimization this fidelity is averaged over 20 repetitions,

and this average is fed into the optimizer. At the end of the optimization an optimal frequency ω_{opt} is returned by the optimizer (see Appendix A).

In Fig. 4, the average values of the fidelity are plotted as a function of discrete time $t = k(nT_{opt})$, where k is an integer number, $T_{opt} = 2\pi/\omega_{opt}$ and ω_{opt} is the optimized frequency obtained after 15 iterations. It can be observed that the average fidelity is above 70% for a very long time for both the period-doubling ($n = 2$) and period-quadrupling ($n = 4$) cases. Without optimization the fidelity drops to almost zero after a few periods of the mirror oscillations. This shows the effectiveness of the Bayesian optimization technique based on a limited number of experimental repetitions to control the true distance h of the atomic cloud to the mirror.
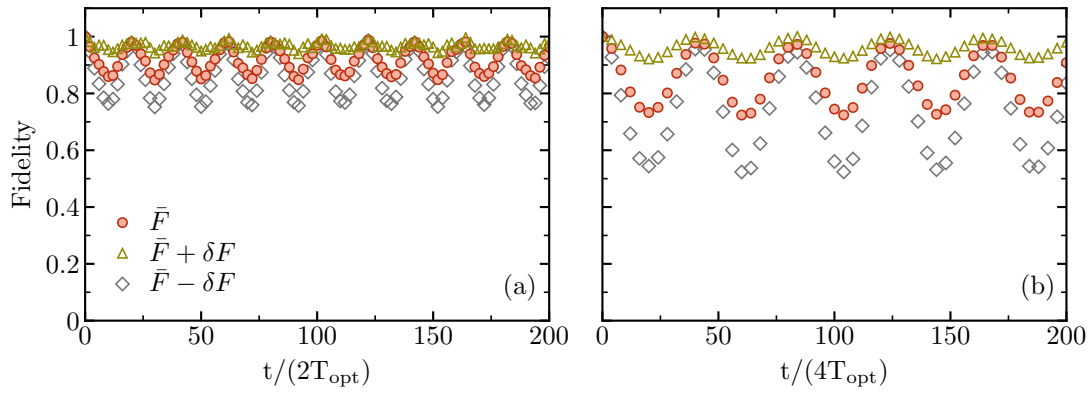
Figure 4. Figure shows fidelity for the optimized frequency $\bar{F} = \langle F_j(\omega_{opt}) \rangle$ averaged over $j = 1, \ldots, 20$ random realizations of the experiment together with $\bar{F} \pm \delta F$, where δF is the standard deviation, at discrete moments of time where $T_{opt} = 2\pi/\omega_{opt}$ — full circles correspond to $\bar{F}$, open triangles to $\bar{F} + \delta F$ and open squares to $\bar{F} - \delta F$. Fifteen iterations of Bayesian optimization are used to obtain optimal ω_{opt}. The left panel corresponds to the period-doubling ($n = 2$) and the right panel to period-quadrupling ($n = 4$) DTCs. The other parameters are the following: $\bar{h} = 12.78$ (31.77), $\delta h = 0.05\bar{h}$ ($0.03\bar{h}$), $\delta\tilde{\omega}_0 = 0.02\tilde{\omega}_0$ ($0.02\tilde{\omega}_0$), $\delta p_0 = 0.1$ (0.05) and $\lambda = 0.12$ (0.12) in the left (right) panel.

5. Quantum many-body fluctuations of discrete time crystals

So far we have performed the analysis of the system within the mean-field approximation, i.e. according to the GP equation (3). These results allowed us to obtain the phase diagrams which determine how strongly one may perturb the system and still DTCs are stable. However, the mean-field approach assumes that time evolution of a Bose system is restricted to the many-body Hilbert subspace of product states, $\phi_0(z_1, t)\phi_0(z_2, t) \ldots \phi_0(z_N, t)$. Interactions between bosons couple the product state subspace to the complementary space and can lead to decay of a DTC. We address this problem in the present section within the Bogoliubov approach [47] in the case of the period-doubling time crystal.

Before we switch to the Bogoliubov description, let us first comment on the behavior of ultra-cold atoms bouncing on an oscillating mirror, when we restrict to the many-body resonant Hilbert subspace [2, 11]. In the case of the $2 : 1$ resonant driving, the resonant Hilbert subspace is spanned by the two Wannier-like wavepackets $w_{1,2}(z, t)$, i.e. the bosonic field operator in (2) is restricted to $\hat{\Psi}(z, t) \approx w_1(z, t)\hat{a}_1 + w_2(z, t)\hat{a}_2$ where $\hat{a}_{1,2}$ are the standard bosonic annihilation operators. The many-body Floquet Hamiltonian (2) in the resonant subspace reads [2]

$$\hat{\mathcal{H}} \approx -\frac{J}{2} \left(\hat{a}_1^\dagger \hat{a}_2 + \hat{a}_2^\dagger \hat{a}_1 \right) + \frac{U_{11} - 2U_{12}}{2} \left(\hat{a}_1^\dagger \hat{a}_1^\dagger \hat{a}_1 \hat{a}_1 + \hat{a}_2^\dagger \hat{a}_2^\dagger \hat{a}_2 \hat{a}_2 \right), \qquad (9)$$

with J and U_{ij} similar to (4). The above Hamiltonian $\hat{\mathcal{H}}$ is identical to the Hamiltonian for bosons in a double well potential within the two-mode approximation [57] — in the present case the two modes are not time-independent functions but the $(2T)$-periodic Wannier wavepackets $w_{1,2}(z, t)$. It is known that the Hamiltonian (9) can be mapped to the Lipkin-Meshkov-Glick model [58]

$$\hat{\mathcal{H}} = J \left(-\hat{S}_x + \frac{\gamma}{N} \hat{S}_z^2 \right), \qquad (10)$$

with a constant term omitted, where the spin operators read

$$\hat{S}_x = \frac{\hat{a}_1^\dagger \hat{a}_2 + \hat{a}_2^\dagger \hat{a}_1}{2}, \qquad \hat{S}_z = \frac{\hat{a}_2^\dagger \hat{a}_2 - \hat{a}_1^\dagger \hat{a}_1}{2}, \qquad (11)$$

and $\gamma = N(U_{11} - 2U_{12})/J \propto g_0 N$. In the limit when $N \to \infty$ but $\gamma = \text{const}$ and $\gamma < -1$ (i.e. for sufficiently strong attractive interactions between bosons), the Lipkin-Meshkov-Glick model reveals a quantum phase transition where the $\mathbb{Z}_2$ symmetry (the $\mathbb{Z}_2$ symmetry means that $\hat{\mathcal{H}}$ commutes with $e^{i\pi \hat{S}_x}$) of the Hamiltonian (10) is spontaneously broken. Then, all the eigenstates of the model for eigenenergies below the so-called symmetry broken edge $-JN/2$ reveal spontaneous breaking of the $\mathbb{Z}_2$ symmetry. The spontaneous breaking of the $\mathbb{Z}_2$ symmetry of the model corresponds to the spontaneous breaking of the time translation symmetry of ultra-cold atoms bouncing on an oscillating mirror which, in the basis of the $(2T)$-periodic Wannier functions $w_{1,2}(z, t)$, are described by the Floquet Hamiltonian (9) [2]. Thus, all Floquet many-body states of the Floquet Hamiltonian (9) with quasi-energies below the symmetry broken edge reveal period-doubling time crystal behaviour.

Even if in the resonant many-body Hilbert subspace the formation of the DTC is clear, there is still a question what happens in the full many-body Hilbert space of the system, i.e. when we take into account that interactions between bosons couple the resonant subspace with the complementary space? It can be addressed by applying the Bogoliubov approach. We use the particle-number-conserving version of the Bogoliubov theory [59] where the bosonic field operator is decomposed into the operator $\hat{a}_0$, corresponding to the condensate mode $\phi_0(z, t)$, and the operator $\delta\hat{\Psi}_\perp(z, t)$ living in the orthogonal subspace, i.e. $\hat{\Psi}(z, t) = \phi_0(z, t)\hat{a}_0 + \delta\hat{\Psi}_\perp(z, t)$. The operator $\delta\hat{\Psi}_\perp(z, t)$ describes quantum many-body fluctuations around a many-body product state. Even

within the Bogoliubov approach, it is not easy to calculate many-body Floquet states. However, it is much easier to investigate how a Bose system evolves in time if it is initially prepared as a perfect BEC. That is, when we start at $t = 0$ with all bosons in a many-body product state $\Phi(z, 0) = \phi_0(z_1, 0)\phi_0(z_2, 0)\ldots\phi_0(z_N, 0)$, we expect that interactions between bosons can lead to quantum depletion of a condensate. Initially we have a perfect condensate and consequently eigenvalues of the reduced single-particle density matrix, $\rho(z, z'; t = 0) = \langle\Phi(0)|\hat{\Psi}^\dagger(z, t = 0)\hat{\Psi}(z', t = 0)|\Phi(0)\rangle$, are all zero except the one corresponding to a condensate mode $\phi_0(z, t)$ which is equal to the total number of particles N. In the course of time evolution, bosons are being depleted from a condensate mode $\phi_0(z, t)$ and start occupying other modes which is indicated by the fact that not only one eigenvalue of the reduced single-particle density matrix is non-zero. In the Bogoliubov approach the total number of bosons $dN(t)$ depleted from the condensate is equal to the sum of the norms of $v_i(z, t)$ components of Bogoliubov modes $[u_i(z, t), v_i(z, t)]$,

$$dN(t) = \sum_i \langle v_i(t)|v_i(t)\rangle. \tag{12}$$

In the particle-number-conserving version of the Bogoliubov theory [59], the modes evolve according to the following linear Bogoliubov-de Gennes equation

$$i\partial_t \begin{bmatrix} u_i \\ v_i \end{bmatrix} = \begin{bmatrix} \hat{Q}\left(H_0 + 2g_0N|\phi_0(z, t)|^2\right)\hat{Q} & g_0N\hat{Q}\phi_0^2(z, t)\hat{Q}^* \\ -g_0N\hat{Q}^*\phi_0^{*2}(z, t)\hat{Q} & -\hat{Q}^*\left(H_0 + 2g_0N|\phi_0(z, t)|^2\right)\hat{Q}^* \end{bmatrix} \begin{bmatrix} u_i \\ v_i \end{bmatrix}, \tag{13}$$

where $\phi_0(z, t)$ fulfills the GP equation (3), $\hat{Q} = 1 - |\phi_0(t)\rangle\langle\phi_0(t)|$ and $\hat{Q}^* = 1 - |\phi_0^*(t)\rangle\langle\phi_0^*(t)|$. Initial Bogoliubov modes allow us to define an initial many-body state of N bosons. If at $t = 0$ we choose $[u_i(z, 0), v_i(z, 0)] = [\chi_i(z), 0]$ (where $\langle\chi_i|\chi_j\rangle = \delta_{ij}$ and $\langle\chi_i|\phi_0(0)\rangle = 0$) and the Bogoliubov vacuum state as the initial state [60], we deal with the many-body state which is a perfect condensate [60], i.e. no bosons are initially depleted $dN(0) = 0$. The choice of $\chi_i(z)$ is arbitrary but if we do our best and choose $\chi_i(z)$ optimally adapted to a given problem, we will have to evolve a small number of the Bogliubov modes only in order to get the converged result for the total number of depleted bosons $dN(t)$. In the case of the $2 : 1$ resonant bouncing of ultra-cold atoms on an oscillating atom mirror, we start with $\phi_0(z, 0)$ as the Gaussian state (5) and $\chi_i(z)$ as eigenstates of the Hartree-Fock Hamiltonian $H_{\text{HF}} = -\frac{1}{2}\partial_z^2 + z + \lambda z + 2g_0N|\phi_0(z, 0)|^2$ where contributions to the condensate mode are subtracted, i.e. $\langle\chi_i|\phi_0(0)\rangle = 0$ and $\chi_i(z)$ are corrected so that $\langle\chi_i|\chi_j\rangle = \delta_{ij}$.

Evolving the condensate mode $\phi_0(z, t)$ according to the GP equation (3) and the Bogoliubov modes $[u_i(z, t), v_i(z, t)]$ according to the Bogolibov-de Gennes equations (13) we can obtain the reduced single-particle density matrix at any time t and diagonalize it,

$$\rho(z, z'; t) \approx N\phi_0^*(z, t)\phi_0(z', t) + \sum_i v_i(z, t)v_i^*(z', t)$$

$$= N\phi_0^*(z, t)\phi_0(z', t) + \sum_{j=1}^{\infty} dN_j(t)\,\phi_j^*(z, t)\phi_j(z', t). \tag{14}$$

Figure 5a shows how the total depletion changes in time. It turns out that it is entirely determined by only one eigenmode of the single-particle density matrix, i.e. $dN(t) = \sum_j dN_j(t) \approx dN_1(t)$. After a long time of 1000 bounces of ultra-cold atoms on an oscillating mirror, i.e. at $t_f = 1999T$, the total depletion is of the order of one atom only, $dN(t_f) \approx 1.6$. It depends on the product $g_0 N$ because the Bogoliubov-de Gennes equations (13) depend on $g_0 N$. In the experiment a typical total number of atoms is of the order $N \approx 10^4$ which implies that for $g_0 N = -0.02$ chosen here, $dN(t_f)/N$ is negligible and the DTC is stable and resistant to quantum many-body fluctuations at least in a time scale that we have investigated here. The latter is much longer than expected duration of the experiment [11].
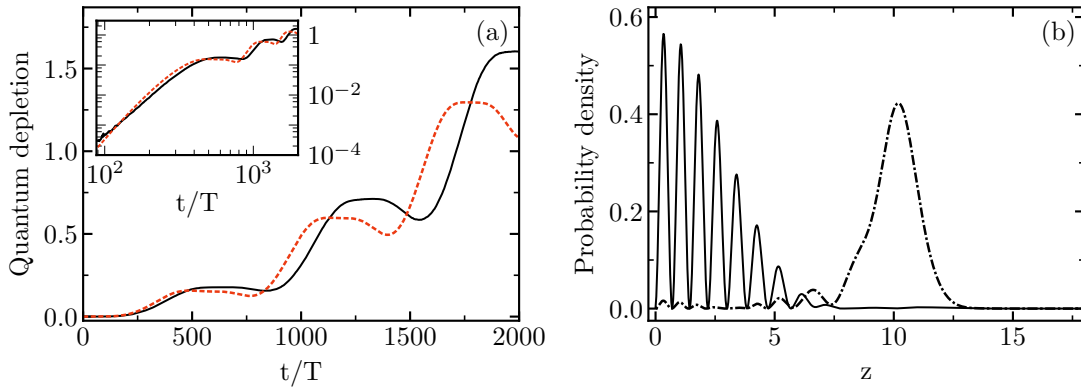
Figure 5. Left panel: black solid line shows the average number of atoms $dN(t)$ depleted from the condensate wavefunction $\phi_0(z, t)$. Initially $\phi_0(z, t)$ corresponds to the Gaussian wavepacket (5) and its time evolution $\phi_0(z, t)$, according to the GP equation (3), describes the period-doubling time crystal. The total depletion of the condensate is dominated by a single eigenmode $\phi_1(z, t)$ of the reduced single-particle density matrix (14), i.e. $dN(t) \approx dN_1(t)$, because other eigenvalues $dN_{j>1}(t) \le 6 \times 10^{-3}$. Red dashed line shows the condensate depletion obtained with the help of the two-mode approach (9). Inset presents the total depletion $dN(t)$ in the log-log-scale indicating the initial algebraic increase of the depletion. Right panel: probability densities of the condensate mode $|\phi_0(z, t)|^2$ (black solid line) and the dominant mode $|\phi_1(z, t)|^2$ (dotted-dashed line) at the final moment of the time evolution, i.e. at $t = 1999T$ — both $\phi_0(z, t)$ and $\phi_1(z, t)$ are normalized to unity. The parameters of the mirror oscillations are: $\lambda = 0.12$ and $\omega = 1.4$. The total evolution time $1999T$ corresponds to two tunneling periods of non-interacting atoms between the two Wannier wavepackets $w_{1,2}$ which is $2\pi/J$ where $J = 7.26 \times 10^{-4}$, cf. (9). The parameters of the two-mode Hamiltonian (9) are $U/g_0 = 0.23$ and $U_{12}/g_0 = 0.05$, and the interaction strength is chosen so that $g_0 N = -0.02$. The two-mode results are obtained for $N = 600$ but they remain the same if N is greater.

Figure 5b presents probability densities of the condensate mode $|\phi_0(z, t_f)|^2$ and the dominant mode $|\phi_1(z, t_f)|^2$ of the reduced single-particle density matrix (14). It turns out that $|\langle \phi_0(t_f \pm T)|\phi_1(t_f)\rangle|^2 \approx 0.87 \pm 0.02$ what implies that atoms depleted from the condensate occupy the wavepacket that travels along the $2:1$ resonant orbit but is delayed with respect to the condensate mode by the period T of the mirror oscillations. Thus, the many-body evolution of the system is restricted to two modes and these modes

are similar to the modes $w_1(z,t)$ and $w_2(z,t)$ used to define the resonant many-body Hilbert subspace, cf. (9).

Let us compare the quantum many-body effects in the time crystal evolution obtained within the Bogoliubov approach and by means of the two-mode Hamiltonian (9). In the two-mode case, the perfect BEC with all atoms occupying the mode $w_1(z,t)$ corresponds to $|N,0\rangle$ and it is the initial state we choose in the two-mode description. At $t = 0$ the quantum depletion of the condensate is zero but because the initial state is not an eigenstate of the Hamiltonian (9), the depletion increases in time which is shown in Fig. 5a. Despite the fact that in the Bogoliubov description, the initial condensate wavefunction $\phi_0(z,0)$ is not exactly the mode $w_1(z,0)$ (i.e. $\phi_0(z,0)$ is the Gaussian approximation of the mode $w_1(z,t)$ only), the results for the quantum depletion obtained with the help of the both methods follow each other quite well. The results of the two-mode approach correspond to $N = 600$ but they are the same for any $N > 600$ provided $g_0 N = -0.02$. The two-mode description allows us also to investigate what happens in an extremely long time scale. It turns out that at $t \approx 500 T \sqrt{N}$, the depletion saturates at $dN \approx 0.02N$ and next, for much longer time evolution, the N-body system shows a revival and returns to the initial perfect BEC.

The initial BEC states used in the Bogoliubov description and in the two-mode approach are generic uncorrelated states of the resonantly driven many-body system. The presented results of the many-body time evolution of these states show that heating effects are negligible.

6. Conclusion

The intriguing possibility of studying novel quantum many-body phenomena in the time domain relies on realizing n-tupling DTC with large n, which so far has eluded any experimental observations. Adopting a model of ultra-cold atoms bouncing on an oscillating mirror that can be experimentally realized, we obtain the optimal conditions required for the initial state preparation of the system. Such optimization allows us to control and manipulate the system despite the experimental uncertainties and imperfections. The Bayesian method used here to obtain the phase diagram efficiently for small n can be naturally extended for large n-tupling DTC. This provides invaluable information for the experimentalists as it provides a well defined criterion for distinguishing the symmetry broken phase from the unbroken phase. Finally, our analysis of quantum many-body fluctuations that go beyond the mean-field approximation, clearly indicates that DTCs realized in our model do not show any signs of heating on long time scale — much longer than the duration of experiments. Thus, the integrability of the periodically driven single-particle system that reveals non-linear resonances is inherited by the many-body counterpart if the interactions between particles are weak but still sufficiently strong to form DTCs. In summary, this work is definitely a step towards bridging the gap between theory and experiments on n-tupling DTC with the possibility of using optimal control in the experimental realisation of

DTCs in ultra-cold systems.

Acknowledgements

Appendix A. Bayesian optimisation

A typical optimization problem involves maximizing a figure of merit $F(\mathbf{x})$ with respect to its input parameters $\mathbf{x}$,

$$\mathbf{x}^{\text{opt}} = \arg\max_{\mathbf{x}} \ F(\mathbf{x}). \tag{A.1}$$

In general, $\mathbf{x}$ can be a $\mathcal{N}$-dimensional vector where $\mathcal{N}$ is the total number of parameters. In order to obtain the optimum solution $\mathbf{x}^{\text{opt}}$, one has to evaluate the figure of merit multiple times with $F(\mathbf{x}_i)$ representing the result of i$^{\text{th}}$ evaluation. The dependence of the figure of merit $F(\mathbf{x})$ on $\mathbf{x}$ defines the optimization landscape which can often be non trivial. One way to perform this optimization task is by means of gradient methods. However, as it is the case here, analytical gradient of $F(\mathbf{x})$ are not available, and approximations of these gradients by finite differences require extra numerical or experimental effort. Moreover this approach is limited by the presence of local extremum in the optimization landscape.

Keeping this in mind, we resort to a non-gradient based optimization scheme, namely Bayesian optimization, which has been extremely efficient in terms of the number of evaluations needed to obtain close-to-optimum solutions [61–64] even in the presence of noise in the input parameters [65], or in the evaluation of the figure of merit [66]. Bayesian optimization is a technique that adopts a probabilistic approach towards optimization. It has essentially three steps: first, it approximates the unknown optimization landscape $F(\mathbf{x})$ with well-behaved random functions f with prior distribution, that is before obtaining any evaluation, $p(f)$. Given M evaluations of the figure of merit denoted $\mathbf{y}_M = [F(\mathbf{x}_1), \ldots F(\mathbf{x}_M)]$, this distribution is updated to incorporate the data acquired by means of Bayes' rule

$$p(f|\mathbf{y}_M) = \frac{p(f)p(\mathbf{y}_M|f)}{p(\mathbf{y}_M)}, \tag{A.2}$$

The final step involves deciding, based on this model f, which parameters to evaluate next. A short-sighted strategy would consist on selecting the next set of parameters $\mathbf{x}_{i+1}$ where the model takes its maximal value. However, since the model f is only an approximation of the true optimization landscape F, there is also incentive to explore other regions of the parameter space where few evaluations have been recorded.

These two conflicting aspects, known as exploration-exploitation, are incorporated in Bayesian optimization by means of an acquisition function which values both the search for a maxima and also encourage exploration. The next set of parameters to evaluate is then chosen such that it maximizes this acquisition function. For example the upper confidence bound acquisition function, which was used in this work, is defined as

$$\alpha_{UCB}(\mathbf{x}) = \mu_f(\mathbf{x}) + k\sigma_f(\mathbf{x}). \tag{A.3}$$

$\mu_f(\mathbf{x})$ and $\sigma_f(\mathbf{x})$ are respectively the mean and the standard deviation of the predictive distribution given in Eq. (A.2). The parameter k determines the exploration-exploitation balance with higher values of k corresponding to more exploration. More details about the specificity of building and updating the probabilistic models within Bayesian optimization can be found in Refs. [67–70].

References

[1] Frank Wilczek. Quantum time crystals. *Phys. Rev. Lett.*, 109:160401, Oct 2012.

[2] Krzysztof Sacha. Modeling spontaneous breaking of time-translation symmetry. *Phys. Rev. A*, 91:033617, Mar 2015.

[3] Vedika Khemani, Achilleas Lazarides, Roderich Moessner, and S. L. Sondhi. Phase structure of driven quantum systems. *Phys. Rev. Lett.*, 116:250401, Jun 2016.

[4] Dominic V. Else, Bela Bauer, and Chetan Nayak. Floquet time crystals. *Phys. Rev. Lett.*, 117:090402, Aug 2016.

[5] N. Y. Yao, A. C. Potter, I.-D. Potirniche, and A. Vishwanath. Discrete time crystals: Rigidity, criticality, and realizations. *Phys. Rev. Lett.*, 118:030401, Jan 2017.

[6] Angelo Russomanno, Fernando Iemini, Marcello Dalmonte, and Rosario Fazio. Floquet time crystal in the lipkin-meshkov-glick model. *Phys. Rev. B*, 95:214307, Jun 2017.

[7] Zongping Gong, Ryusuke Hamazaki, and Masahito Ueda. Discrete time-crystalline order in cavity and circuit qed systems. *Phys. Rev. Lett.*, 120:040404, Jan 2018.

[8] Biao Huang, Ying-Hai Wu, and W. Vincent Liu. Clean floquet time crystals: Models and realizations in cold atoms. *Phys. Rev. Lett.*, 120:110603, Mar 2018.

[9] F. Iemini, A. Russomanno, J. Keeling, M. Schirò, M. Dalmonte, and R. Fazio. Boundary time crystals. *Phys. Rev. Lett.*, 121:035301, Jul 2018.

[10] Tian-Sheng Zeng and D. N. Sheng. Prethermal time crystals in a one-dimensional periodically driven floquet system. *Phys. Rev. B*, 96:094202, Sep 2017.

[11] Krzysztof Giergiel, Arkadiusz Kosior, Peter Hannaford, and Krzysztof Sacha. Time crystals: Analysis of experimental conditions. *Phys. Rev. A*, 98:013613, Jul 2018.

[12] Krzysztof Sacha and Jakub Zakrzewski. Time crystals: a review. *Reports on Progress in Physics*, 81(1):016401, nov 2017.

[13] Kaoru Mizuta, Kazuaki Takasan, Masaya Nakagawa, and Norio Kawakami. Spatial-translation-induced discrete time crystals. *Phys. Rev. Lett.*, 121:093001, Aug 2018.

[14] L. Liao, J. Smits, P. van der Straten, and H. T. C. Stoof. Dynamics of a space-time crystal in an atomic bose-einstein condensate. *Phys. Rev. A*, 99:013625, Jan 2019.

[15] F. M. Gambetta, F. Carollo, M. Marcuzzi, J. P. Garrahan, and I. Lesanovsky. Discrete time crystals in the absence of manifest symmetries or disorder in open quantum systems. *Phys. Rev. Lett.*, 122:015701, Jan 2019.

[16] Vedika Khemani, Roderich Moessner, and S. L. Sondhi. A Brief History of Time Crystals. *arXiv e-prints*, page arXiv:1910.10745, October 2019.

[17] Jayson G. Cosme, Jim Skulte, and Ludwig Mathey. Time crystals in a shaken atom-cavity system. *Phys. Rev. A*, 100:053615, Nov 2019.

[18] J Zhang, PW Hess, A Kyprianidis, P Becker, A Lee, J Smith, G Pagano, I-D Potirniche, Andrew C Potter, A Vishwanath, et al. Observation of a discrete time crystal. *Nature*, 543(7644):217, 2017.

[19] Soonwon Choi, Joonhee Choi, Renate Landig, Georg Kucsko, Hengyun Zhou, Junichi Isoya, Fedor Jelezko, Shinobu Onoda, Hitoshi Sumiya, Vedika Khemani, et al. Observation of discrete time-crystalline order in a disordered dipolar many-body system. *Nature*, 543(7644):221, 2017.

[20] Soham Pal, Naveen Nishad, T. S. Mahesh, and G. J. Sreejith. Temporal order in periodically driven spins in star-shaped clusters. *Phys. Rev. Lett.*, 120:180602, May 2018.

[21] Jared Rovny, Robert L. Blum, and Sean E. Barrett. Observation of discrete-time-crystal signatures in an ordered dipolar many-body system. *Phys. Rev. Lett.*, 120:180603, May 2018.

[22] Jared Rovny, Robert L. Blum, and Sean E. Barrett. ^{31}P nmr study of discrete time-crystalline signatures in an ordered crystal of ammonium dihydrogen phosphate. *Phys. Rev. B*, 97:184301, May 2018.

[23] J. Smits, L. Liao, H. T. C. Stoof, and P. van der Straten. Observation of a space-time crystal in a superfluid quantum gas. *Phys. Rev. Lett.*, 121:185301, Oct 2018.

[24] Patrick Bruno. Impossibility of spontaneously rotating time crystals: A no-go theorem. *Phys. Rev. Lett.*, 111:070402, Aug 2013.

[25] Andrzej Syrwid, Jakub Zakrzewski, and Krzysztof Sacha. Time crystal behavior of excited eigenstates. *Phys. Rev. Lett.*, 119:250602, Dec 2017.

[26] Haruki Watanabe and Masaki Oshikawa. Absence of quantum time crystals. *Phys. Rev. Lett.*, 114:251603, Jun 2015.

[27] Haruki Watanabe, Masaki Oshikawa, and Tohru Koma. Proof of the absence of long-range temporal orders in gibbs states, 2019.

[28] Valerii K. Kozin and Oleksandr Kyriienko. Quantum time crystals from hamiltonians with long-range interactions. *Phys. Rev. Lett.*, 123:210602, Nov 2019.

[29] Vedika Khemani, Roderich Moessner, and S. L. Sondhi. Comment on "Quantum Time Crystals from Hamiltonians with Long-Range Interactions". *arXiv e-prints*, page arXiv:2001.11037, January 2020.

[30] Federica Maria Surace, Angelo Russomanno, Marcello Dalmonte, Alessandro Silva, Rosario Fazio, and Fernando Iemini. Floquet time crystals in clock models. *Phys. Rev. B*, 99:104303, Mar 2019.

[31] Paweł Matus and Krzysztof Sacha. Fractional time crystals. *Phys. Rev. A*, 99:033626, Mar 2019.

[32] Andrea Pizzi, Johannes Knolle, and Andreas Nunnenkamp. Period-n discrete time crystals and quasicrystals with ultracold bosons. *Phys. Rev. Lett.*, 123:150601, Oct 2019.

[33] Andrea Pizzi, Johannes Knolle, and Andreas Nunnenkamp. Higher-order and fractional discrete time crystals in clean long-range interacting systems. *arXiv e-prints*, page arXiv:1910.07539, October 2019.

[34] Eran Lustig, Yonatan Sharabi, and Mordechai Segev. Topological aspects of photonic time crystals. *Optica*, 5(11):1390–1395, Nov 2018.

[35] Krzysztof Giergiel, Alexandre Dauphin, Maciej Lewenstein, Jakub Zakrzewski, and Krzysztof Sacha. Topological time crystals. *New Journal of Physics*, 21(5):052003, may 2019.

[36] Tongcang Li, Zhe-Xuan Gong, Zhang-Qi Yin, H. T. Quan, Xiaobo Yin, Peng Zhang, L.-M. Duan, and Xiang Zhang. Space-time crystals of trapped ions. *Phys. Rev. Lett.*, 109:163001, Oct 2012.

[37] Yi Huang, Tongcang Li, and Zhang-qi Yin. Symmetry-breaking dynamics of the finite-size lipkin-meshkov-glick model near ground state. *Phys. Rev. A*, 97:012115, Jan 2018.

[38] Krzysztof Giergiel, Artur Miroszewski, and Krzysztof Sacha. Time crystal platform: From quasicrystal structures in time to systems with exotic interactions. *Phys. Rev. Lett.*, 120:140401, Apr 2018.

[39] Krzysztof Giergiel, Arkadiusz Kuroś, and Krzysztof Sacha. Discrete time quasicrystals. *Phys. Rev. B*, 99:220303, Jun 2019.

[40] Krzysztof Sacha. Anderson localization and mott insulator phase in the time domain. *Scientific*

reports, 5:10787, 2015.

[41] Krzysztof Sacha and Dominique Delande. Anderson localization in the time domain. *Phys. Rev. A*, 94:023633, Aug 2016.

[42] Dominique Delande, Luis Morales-Molina, and Krzysztof Sacha. Three-dimensional localized-delocalized anderson transition in the time domain. *Phys. Rev. Lett.*, 119:230404, Dec 2017.

[43] Marcin Mierzejewski, Krzysztof Giergiel, and Krzysztof Sacha. Many-body localization caused by temporal disorder. *Phys. Rev. B*, 96:140201, Oct 2017.

[44] Arkadiusz Kosior and Krzysztof Sacha. Dynamical quantum phase transitions in discrete time crystals. *Phys. Rev. A*, 97:053621, May 2018.

[45] Arkadiusz Kosior, Andrzej Syrwid, and Krzysztof Sacha. Dynamical quantum phase transitions in systems with broken continuous time and space translation symmetries. *Phys. Rev. A*, 98:023612, Aug 2018.

[46] Krzysztof Giergiel, Tien Tran, Ali Zaheer, Arpana Singh, Andrei Sidorov, Krzysztof Sacha, and Peter Hannaford. Creating big time crystals with ultracold atoms. *arXiv e-prints*, page arXiv:2004.00755, April 2020.

[47] C. Pethick and H. Smith. *Bose-Eistein condensation in dilute gases*. Cambridge University Press, Cambridge, England, 2002.

[48] Martin Holthaus and Michael E. Flatté. Subharmonic generation in quantum systems. *Physics Letters A*, 187(2):151 – 156, 1994.

[49] Michael E Flatté and Martin Holthaus. Classical and quantum dynamics of a periodically driven particle in a triangular well. *Annals of Physics*, 245(1):113 – 146, 1996.

[50] Andreas Buchleitner, Dominique Delande, and Jakub Zakrzewski. Non-dispersive wave packets in periodically driven quantum systems. *Physics reports*, 368(5):409–547, 2002.

[51] A.J. Lichtenberg and M.A. Lieberman. *Regular and chaotic dynamics*. Applied mathematical sciences. Springer-Verlag, 1992.

[52] G.P. Berman and G.M. Zaslavsky. Theory of quantum nonlinear resonance. *Physics Letters A*, 61(5):295–296, 1977.

[53] Lingzhen Guo, Michael Marthaler, and Gerd Schön. Phase space crystals: A new way to create a quasienergy band structure. *Phys. Rev. Lett.*, 111:205303, Nov 2013.

[54] Lingzhen Guo and Michael Marthaler. Synthesizing lattice structures in phase space. *New Journal of Physics*, 18(2):023006, 2016.

[55] Lingzhen Guo, Modan Liu, and Michael Marthaler. Effective long-distance interaction from short-distance interaction in a periodically driven one-dimensional classical system. *Phys. Rev. A*, 93:053616, May 2016.

[56] Liang Pengfei, Marthaler Michael, and Lingzhen Guo. Floquet many-body engineering: topology and many-body physics in phase space lattices. *New Journal of Physics*, 20(2):023043, 2018.

[57] G. J. Milburn, J. Corney, E. M. Wright, and D. F. Walls. Quantum dynamics of an atomic bose-einstein condensate in a double-well potential. *Phys. Rev. A*, 55:4318–4324, Jun 1997.

[58] Pedro Ribeiro, Julien Vidal, and Rémy Mosseri. Exact spectrum of the lipkin-meshkov-glick model in the thermodynamic limit and finite-size corrections. *Phys. Rev. E*, 78:021106, Aug 2008.

[59] Y. Castin and R. Dum. Low-temperature bose-einstein condensates in time-dependent traps: Beyond the $u(1)$ symmetry-breaking approach. *Phys. Rev. A*, 57:3008–3021, Apr 1998.

[60] Jacek Dziarmaga and Krzysztof Sacha. Images of a bose–einstein condensate: diagonal dynamical bogoliubov vacuum. *Journal of Physics B: Atomic, Molecular and Optical Physics*, 39(1):57–68, dec 2005.

[61] P. B. Wigley, P. J. Everitt, A. van den Hengel, J. W. Bastian, M. A. Sooriyabandara, G. D. McDonald, K. S. Hardman, C. D. Quinlivan, P. Manju, C. C. N. Kuhn, I. R. Petersen, A. N. Luiten, J. J. Hope, N. P. Robins, and M. R. Hush. Fast machine-learning online optimization of ultra-cold-atom experiments. *Sci. Rep.*, 6(1):25890, May 2016.

[62] D. Zhu, N. M. Linke, M. Benedetti, K. A. Landsman, N. H. Nguyen, C. H. Alderete, A. Perdomo-Ortiz, N. Korda, A. Garfoot, C. Brecque, L. Egan, O. Perdomo, and C. Monroe. Training of

Quantum Circuits on a Hybrid Quantum Computer. *arXiv:1812.08862*, 2018.

[63] Bryce M. Henson, Dong K. Shin, Kieran F. Thomas, Jacob A. Ross, Michael R. Hush, Sean S. Hodgman, and Andrew G. Truscott. Approaching the adiabatic timescale with machine learning. *Proceedings of the National Academy of Sciences of the United States of America*, 115(52):13216–13221, 2018.

[64] Ippei Nakamura, Atsunori Kanemura, Takumi Nakaso, Ryuta Yamamoto, and Takeshi Fukuhara. Non-standard trajectories found by machine learning for evaporative cooling of 87 Rb atoms . *Optics Express*, 27(15):20435, 2019.

[65] Rick Mukherjee, Frederic Sauvage, Harry Xie, Robert Löw, and Florian Mintert. Preparation of ordered states in ultra-cold gases using Bayesian optimization. *arXiv e-prints*, page arXiv:2001.03520, January 2020.

[66] Frederic Sauvage and Florian Mintert. Optimal quantum control with poor statistics. *arXiv e-prints*, page arXiv:1909.01229, Sep 2019.

[67] Eric Brochu, Vlad M Cora, and Nando De Freitas. A tutorial on bayesian optimization of expensive cost functions, with application to active user modeling and hierarchical reinforcement learning. *arXiv:1012.2599*, 2010.

[68] Jasper Snoek, Hugo Larochelle, and Ryan P Adams. Practical bayesian optimization of machine learning algorithms. In *Advances in neural information processing systems*, pages 2951–2959, 2012.

[69] Peter I Frazier. A tutorial on bayesian optimization. *arXiv:1807.02811*, 2018.

[70] Bobak Shahriari, Kevin Swersky, Ziyu Wang, Ryan P Adams, and Nando De Freitas. Taking the human out of the loop: A review of bayesian optimization. *Proceedings of the IEEE*, 104(1):148–175, 2015.